

Microwave-induced resistance oscillations and zero-resistance states in 2D electron systems with two occupied subbands

J. Iñarrea¹ and G. Platero²

¹*Escuela Politécnica Superior, Universidad Carlos III, Leganes, Madrid, 28911, Spain*

²*Instituto de Ciencia de Materiales, CSIC, Cantoblanco, Madrid, 28049, Spain*

(Dated: July 27, 2018)

We report on theoretical studies of recently discovered microwave-induced resistance oscillations and zero resistance states in Hall bars with two occupied subbands. In the same results, resistance presents a peculiar shape which appears to have a built-in interference effect not observed before. We apply the microwave-driven electron orbit model, which implies a radiation-driven oscillation of the two-dimensional electron system. Thus, we calculate different intra and inter-subband electron scattering rates and times that are revealing as different microwave-driven oscillations frequencies for the two electronic subbands. Through scattering, these subband-dependent oscillation motions interfere giving rise to a striking resistance profile. We also study the dependence of irradiated magnetoresistance with power and temperature. Calculated results are in good agreement with experiments.

PACS numbers:

I. INTRODUCTION

Transport excited by radiation in a two-dimensional electron system (2DES) is currently a central topic from experimental and theoretical standpoints¹. The interest is focussed not only on the basic explanation of a physical effect but also on its potential applications. In the last decade it was discovered that when a Hall bar (a 2DES with a uniform and perpendicular magnetic field (B)) is irradiated with microwaves, some unexpected effects are revealed, deserving special attention from the condensed matter community: microwave-induced (MW) resistance oscillations (MIRO) and zero resistance states (ZRS)²⁻⁴. These remarkable effects show up at low B and high mobility samples, specially ZRS where ultraclean samples are needed. Different theories have been proposed to explain these striking effects⁵⁻¹¹ but the physical origin is still being questioned. To shed some light on the physics behind them, a great effort has been made, specially from the experimental side, growing better samples, adding new features and different probes to the basic experimental setup, etc.¹²⁻²⁷. Of course the experimental results always mean a real challenge for the existent theoretical models. Thus, a comparison of experiment with theory could help to identify the importance of the invoked mechanisms in these theories.

One of the most interesting setups, carried out recently, consists in using samples with two or three occupied subbands²³. These samples are either based in a double quantum well structure or just one single but wide quantum well. The main difference in the longitudinal magnetoresistance (R_{xx}) of a two-subband sample is the presence of magneto-intersubband oscillations (MISO)²⁸. These oscillations occur due to periodic modulation of the probability of transitions through elastic scattering between Landau levels (LL) of different subband. The MISO peaks corresponds to the subband alignment condition $\Delta = n\hbar\omega_c$, where Δ is the subband separation and

ω_c the cyclotron frequency. Because of elastic scattering of electrons between LL of different subband, the probability rate is maximal under this condition. Under MW irradiation the first experimental results²⁴ of R_{xx} showed the interference of MISO and MIRO without reaching the ZRS regime. Later on, further experiments realized at higher MW intensities and mobility samples, showed the MW-response to evolve into zero resistance states for the first time in a two occupied subband sample²³. In the same experiment²³ it was also observed a peculiar R_{xx} profile with different features, regarding the one-subband case²⁻⁴, affecting only valleys and peaks of MIRO's in a surprising regular way. Thus, in valleys we observe two nearly symmetric shoulders, one at each side of minimum which could correspond to a more intense transport through the sample. On the other hand, in the peaks we observe narrower profiles, regarding again the one subband case, meaning a smaller transport.

In this article, we theoretically study magnetoresistance of a Hall bar being illuminated with MW radiation when two electronic subbands participate in the transport. We apply the theory developed by the authors, *the MW-driven electron orbits model*^{5,32-34}, which we extend to a two-subband scenario. According to this theory, when a Hall bar is illuminated, the electron orbit centers of the Landau states perform a classical trajectory consisting in a harmonic motion along the direction of the current. Thus, the 2DES moves periodically at the MW frequency altering dramatically the scattering conditions and giving rise eventually to MIRO and ZRS. In some cases the transport is reinforced producing MW-induced R_{xx} peaks; in others, transport is weakened giving rise to valleys. In a double subband scenario the situation gets more complicated but with a richer physics. On the one hand, due to the presence of MW, we have two 2DES (two subbands) moving harmonically at the MW-frequency. On the other hand, we have two possible scattering processes with charged impurities: intra and

II. THEORETICAL MODEL

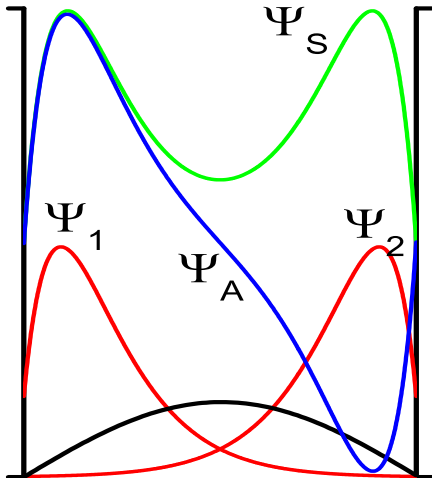


FIG. 1: Schematic diagram for the wide quantum well and the corresponding electronic wave functions. Ψ_1 and Ψ_2 are the individual Fang-Howard wave functions for the left and right triangular-like built-in potential wells. Ψ_S and Ψ_A are the symmetric and antisymmetric wave functions of the wide quantum well. The quantum well has a width of 45nm as in the experiments.

inter-subband. We then calculate the two corresponding elastic impurity scattering rates, obtaining that the intra is, approximately, three times larger than the inter. This means first, that the current is mainly supported by intra-subband scattering processes. Secondly and more important, the competition between intra and inter-subband scattering events under the presence of radiation alters significantly the transport properties of the sample. This is reflected in the R_{xx} profile through a strong and peculiar interference effect. As in experiments, our calculated results recover the presence of new features regularly spaced through the whole MIRO's profile, mainly two shoulders at minima and narrower peaks. We identify such features with situations where the interference is constructive and the current is reinforced (shoulders around minima) meanwhile in other cases the interference is destructive giving rise to a less intense current (thinner peaks). Within the same theory, we have obtained also ZRS in the same position of experiments and with the same MW-frequency dependence. Finally, we have studied the influence of MW-frequency (w), MW-power (P) and temperature (T) on MIRO's of the two subband sample and the obtained results are also in reasonable agreement with experiment²³.

The *MW driven electron orbits model*, was developed to explain the R_{xx} response of an irradiated 2DEG at low B . We first obtain an exact expression of the electronic wave vector for a 2DES in a perpendicular B , a DC electric field and MW radiation which is considered semi-classically. Then, the total hamiltonian H can be written as:

$$\begin{aligned} H &= \frac{P_x^2}{2m^*} + \frac{1}{2}m^*w_c^2(x-X)^2 - eE_{dc}X + \\ &+ \frac{1}{2}m^*\frac{E_{dc}^2}{B^2} - eE_0\cos\omega t(x-X) - \\ &- eE_0\cos\omega tX \\ &= H_1 - eE_0\cos\omega tX \end{aligned} \quad (1)$$

X is the center of the orbit for the electron spiral motion:

$$X = \frac{\hbar k_y}{eB} - \frac{eE_{dc}}{m^*w_c^2} \quad (2)$$

E_0 the intensity for the MW field and E_{dc} is the DC electric field in the x direction. H_1 is the hamiltonian corresponding to a forced harmonic oscillator whose orbit is centered at X . H_1 can be solved exactly^{33,34}, and using this result allows an exact solution for the electronic wave function of H to be obtained^{5,32-35}:

$$\Psi_N(x,t) \propto \phi_n(x-X-x_{cl}(t),t) \quad (3)$$

where ϕ_n is the solution for the Schrödinger equation of the unforced quantum harmonic oscillator, $x_{cl}(t)$ is the classical solution of a forced and damped harmonic oscillator

$$x_{cl} = \frac{eE_o}{m^*\sqrt{(w_c^2 - w^2)^2 + \gamma^4}} \cos\omega t = A \cos\omega t \quad (4)$$

where γ is a phenomenologically-introduced damping factor for the electronic interaction with acoustic phonons.

Then, the obtained wave function is the same as the standard harmonic oscillator where the center is displaced by $x_{cl}(t)$. Thus, the electron orbit centers are not fixed, but they oscillate harmonically at w . This *radiation - driven* behavior will affect dramatically the charged impurity scattering and eventually the conductivity. Thus, we introduce the scattering suffered by the electrons due to charged impurities. If the scattering is weak, we can apply time dependent first order perturbation theory. First, we calculate the impurity scattering rate^{5,32,36} between two *oscillating* Landau states Ψ_N , final state $\Psi_m(x,t)$:

$$W_{n,m} = \lim_{\alpha \rightarrow 0} \frac{d}{dt} \left| \frac{1}{i\hbar} \int_{-\infty}^{t'} \langle \Psi_m(x,t) | V_s | \Psi_n(x,t) \rangle e^{\alpha t} dt \right|^2 \quad (5)$$

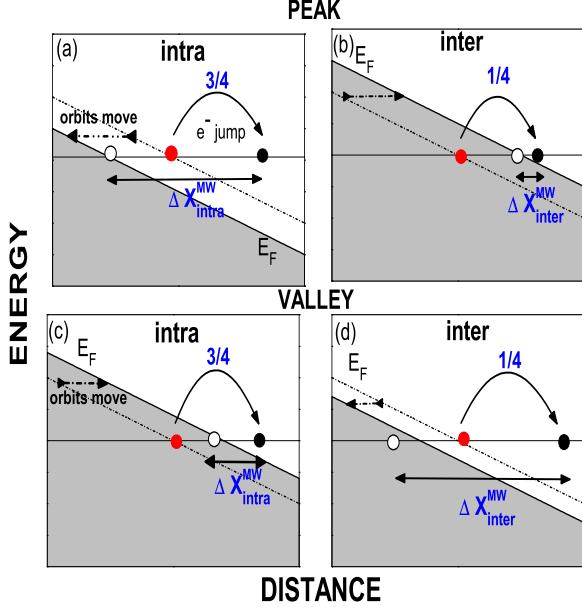


FIG. 2: Schematic diagrams of electronic transport corresponding to peak and valley scenarios and intra and inter-subband scattering types. When the MW field is on, the orbits are not fixed but oscillate at w . In 2a, in the intra-band processes corresponding to peaks, the electronic orbits are going backward giving a larger advanced distance and current. Yet, only 3/4 of these processes develop through this channel. In 2b we represent the inter-subband scattering processes for a peak, where due to the lower scattering time the orbits are now going forwards, yielding a smaller advanced distance and current. According to our calculations they are 1/3 of the total. Summing up all process, the total advance distance is given by $\frac{3}{4}\Delta X_{intra}^{MW} + \frac{1}{4}\Delta X_{inter}^{MW}$. Then, we obtain less current with respect to the one-subband case due to the lower contributions of the inter-subband events. This result correspond to the obtained narrower profiles at maxima. The valleys situation reflected in 2c and 2d, can be explained in similar terms as the peaks but now the discussion and results are going to be the opposite. Then, considering jointly all scattering processes, intra and inter-subband, we obtain, at both sides of minima, more current than the one-subband case due to larger contribution of the inter scattering events. This is the physical origin of the two shoulder that can be observed a both sides at minima.

where V_s is the scattering potential for charged impurities³⁷:

$$V_s = \sum_q \frac{e^2}{2S\epsilon(q + q_0)} \cdot e^{i\vec{q} \cdot \vec{r}} \quad (6)$$

S being the surface of the sample, ϵ the GaAs dielec-

tric constant, and q_0 is the Thomas-Fermi screening constant³⁷.

After some lengthy algebra we arrive at the expressions for the intra-subband $W_{n,m}^{intra}$ and the inter-subband $W_{n,m}^{inter}$ scattering rates:

$$W_{n,m}^{intra} = |F_{intra}|^2 \frac{e^5 n_i S B m^*}{\hbar^4 \epsilon^2 q_0^2} \left[1 + 2 \sum_{s=1}^{\infty} e^{\left(\frac{-s\pi\Gamma}{\hbar w_c}\right)} \right] \quad (7)$$

$$W_{n,m}^{inter} = |F_{inter}|^2 \frac{e^5 n_i S B m^*}{\hbar^4 \epsilon^2 q_0^2} \times \left[1 + 2 \sum_{s=1}^{\infty} e^{\left(\frac{-s\pi\Gamma}{\hbar w_c}\right)} \cos\left(\frac{s2\pi\Delta_{12}}{\hbar w_c}\right) \right] \quad (8)$$

where n_i is the density of impurities, Γ the width of the Landau states, Δ_{12} the subband separation and F_S and F_A are the form factors. To obtain the form factor expressions we have considered, as in experiments²³, a highly doped wide quantum well with $n_i \simeq 9.1 \times 10^{11} \text{cm}^{-2}$. In this type of wells, as more electrons are added, their electrostatic repulsion forces them to pile up near the well sides and the resulting electron charge distribution appears increasingly as bilayer (see Fig. 1). In other words, an effective electrostatic barrier is built up in the middle of the well separating the two electron layers in GaAs. In the case of a double quantum dot the barrier is made of AlGaAs or AlAs. As a result we obtain at each side of the wide quantum well a potential profile similar to the inversion layer of a 2DES that, in a good approximation, can be considered triangular close to the heterojunctions (see Fig. 1). Next, we have to obtain first the corresponding wave functions of these triangular-like built-in potential profiles. Then, due to its great simplicity and as a first approach, we have applied the Fang-Howard variational treatment (see ref.^{37,38}) that proposes as electronic wave function (Fang-Howard wave function):

$$\Psi(z) = \left[\frac{b^3}{2} \right]^{1/2} z e^{-\frac{1}{2}bz}, \quad (9)$$

where b is the corresponding Fang-Howard variational parameter. According to this simple but efficient approach, b results to be mainly dependent on the two-dimensional charged impurity density^{37,38}. Now starting from this variational wave function we can build $\Psi_{S(A)}$ which are the corresponding symmetric (antisymmetric) wave function of the wide quantum well (see Fig. 1). Finally the form factors are obtained:

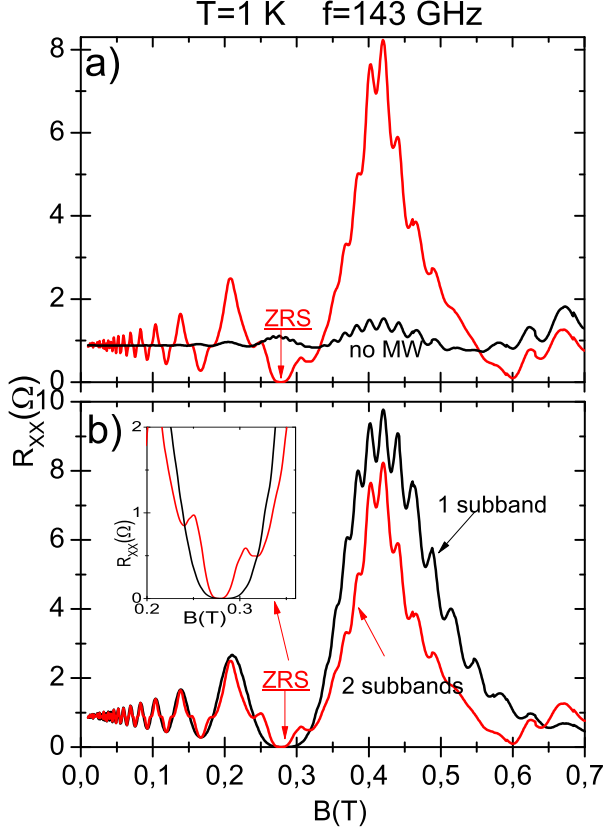


FIG. 3: a) Calculated R_{xx} vs B for dark and MW situations; the ZRS is marked with an arrow. b) Same as a) for 2-subbands and 1-subband. We observe clearly the new features showing up in the 2-subband curve comparing to the 1-subband; shoulders at minima and narrower peaks. In the inset the ZRS region is blown up. Shoulders and narrower peaks are the outcomes of the interference between the intra and inter-subband scattering processes.

$$F_{intra} = \int_0^\infty e^{-q(z-z_i)} \Psi_S^* \Psi_S dz = \frac{e^{-qd}}{2} \left[\left(\frac{b}{b+q} \right)^3 + \left(\frac{b}{b-q} \right)^3 \right] \quad (10)$$

$$F_{inter} = \int_0^\infty e^{-q(z-z_i)} \Psi_S^* \Psi_A dz = \frac{e^{-qd}}{2} \left[\left(\frac{b}{b+q} \right)^3 - \left(\frac{b}{b-q} \right)^3 \right] \quad (11)$$

where q is the electron wave vector exchanged in the scattering. We have supposed a symmetrical delta doping, being d the average separation between the impurities and the 2DES at each side of the wide quantum well, i.e., spacer distance. This distance depends on the sam-

ple. In practical terms it varies between $10nm$ to even larger than $100nm$. In our calculations we have used a numerical value of $d = 70-90nm$. According to the Fang-Howard variational approach^{37,38}, where the parameter b

is given by:

$$b = \left[\frac{33m^*n_i}{8\hbar^2\epsilon} \right]^{1/3} \quad (12)$$

, and applying the experimental sample parameters²³, we have calculated a numerical value for $b \approx 0.25nm^{-1}$. Consequently the average thickness of the triangular wells $\langle z \rangle \simeq 11 - 12nm$, where $\langle z \rangle$ is related with b by $\langle z \rangle = \frac{3}{b}$. Following again with the experimental parameters at hand²³ in terms of impurity density, well thickness, etc., we have made an averaged estimation of the relative values of F_S and F_A resulting in

$$|F_S|^2 = 3.2 \times |F_A|^2 \quad (13)$$

where we have used an average value for $\bar{q} = 0.5nm^{-1}$ that is of the order of the Fermi wave vector in agreement with the experimental impurity density. Substituting the obtained form factors in the scattering rates we can eventually reach averaged values for those rates that result to be related by:

$$\langle W_{n,m}^{intra} \rangle \approx 3 \times \langle W_{n,m}^{inter} \rangle \quad (14)$$

Here we have considered that the cosine average value, $\langle \cos \frac{s2\pi\Delta_{12}}{\hbar w_c} \rangle \rightarrow 0$ for $\Delta_{12} > \hbar w_c$ and we have carried out the sum $\sum_{s=1}^{\infty} e^{\left(\frac{-s\pi\Gamma}{\hbar w_c}\right)} \rightarrow \frac{exp\left(\frac{-s\pi\Gamma}{\hbar w_c}\right)}{1 - exp\left(\frac{-s\pi\Gamma}{\hbar w_c}\right)}$.

Once we know the intra and inter-subband scattering rates, we consider that when an electron undergoes a scattering process jumping from the initial state to the final one, it takes an average time

$$\langle \tau_{intra(inter)} \rangle = \left\langle \frac{1}{W_{n,m}^{intra(inter)}} \right\rangle \quad (15)$$

Following the model described in ref.⁵, we next find the average effective distance advanced by the electron in every scattering jump in the presence of radiation ΔX^{MW} , generalizing the previous results to a two subbands scenario:

$$\Delta X_{intra(inter)}^{MW} = \Delta X^0 + A \cos(w\langle \tau_{intra(inter)} \rangle) \quad (16)$$

where ΔX^0 is the effective distance advanced when there is no MW field present. Applying the important previous result of

$$\langle W_{n,m}^{intra} \rangle \approx 3 \times \langle W_{n,m}^{inter} \rangle \Rightarrow \langle \tau_{intra} \rangle \approx \frac{1}{3} \langle \tau_{inter} \rangle \quad (17)$$

we can write the final expression for the total average distance advance due to both kinds of scattering, intra and inter, ΔX_{total}^{MW} :

$$\Delta X_{total}^{MW} = \Delta X_{intra}^{MW} + \Delta X_{inter}^{MW} \quad (18)$$

$$= A \cos[w\langle \tau_{intra} \rangle] + A \cos[w\langle \tau_{inter} \rangle] \quad (19)$$

$$= A \cos \left[\frac{w}{3} \langle \tau_{inter} \rangle \right] + A \cos[w\langle \tau_{inter} \rangle] \quad (20)$$

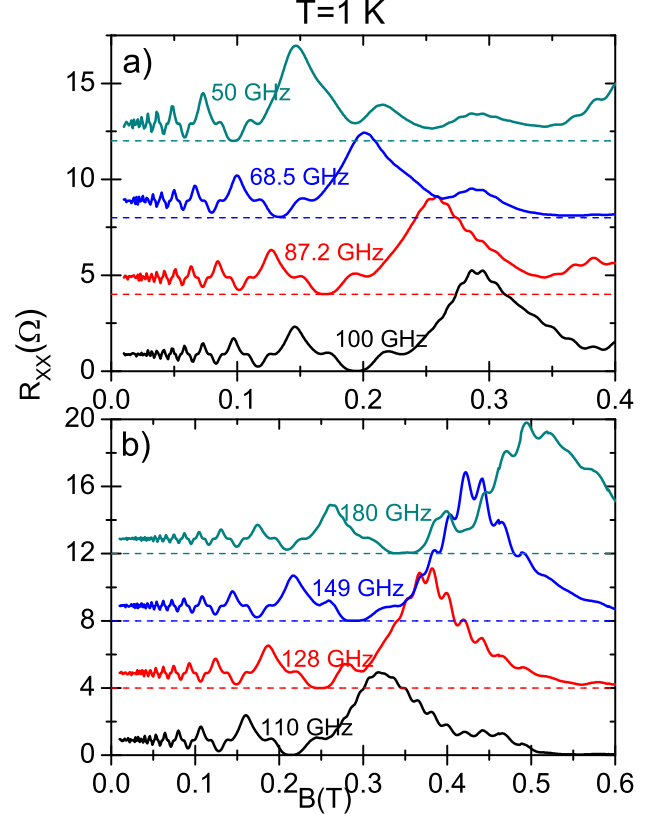


FIG. 4: Calculated R_{xx} vs B for different frequencies. In a) for lower frequencies, from 50 to 100 GHz, and in b) for higher, from 110 to 180 GHz. We observe the presence of ZRS in all curves with shifting positions depending on the frequency and the interference features in peaks and valleys. ZRS positions and shifts are in agreement with experiments^{23,40} and are similar to the one-subband case.

This significantly alters the scattering conditions regarding the one-subband case mainly affecting MIRO's peaks and valleys.

Finally the contributions intra and inter-subband to the longitudinal conductivity can be calculated: $\sigma_{xx} \propto \int dE [(\frac{\Delta X^{MW}}{\tau})_{intra} + (\frac{\Delta X^{MW}}{\tau})_{inter}] (f_i - f_f)$, being f_i and f_f the corresponding distribution functions for the initial and final Landau states respectively and E energy. The obtained final expression for the conductivity is given by:

$$\begin{aligned} \sigma_{xx} = & \frac{6e^7 m^{*2} B n_i S}{\pi \epsilon^2 \hbar^6 q_0} \left[\Delta X^0 + A \cos \frac{1}{3} w \langle \tau_{inter} \rangle \right]^2 \left[1 + 2e^{\frac{-\pi\Gamma}{\hbar\omega_c}} + e^{\frac{-\pi\Gamma}{\hbar\omega_c}} \frac{X_S}{\sinh X_S} \left(\cos \frac{2\pi(E_F - E_1)}{\hbar\omega_c} + \cos \frac{2\pi(E_F - E_2)}{\hbar\omega_c} \right) \right] \\ & + \frac{2e^7 m^{*2} B n_i S}{\pi \epsilon^2 \hbar^6 q_0} \left[\Delta X^0 + A \cos w \langle \tau_{inter} \rangle \right]^2 \left[1 + 2e^{\frac{-\pi\Gamma}{\hbar\omega_c}} \cos \frac{2\pi\Delta_{12}}{\hbar\omega_c} + e^{\frac{-\pi\Gamma}{\hbar\omega_c}} \frac{X_S}{\sinh X_S} \left(\cos \frac{2\pi(E_F - E_1)}{\hbar\omega_c} + \cos \frac{2\pi(E_F - E_2)}{\hbar\omega_c} \right) \right] \end{aligned} \quad (21)$$

where $X_S = \frac{2\pi^2 k_B T}{\hbar\omega_c}$ and E_1 and E_2 are the energies of the first and the second subband respectively. Finally, to obtain R_{xx} we use the relation $R_{xx} = \frac{\sigma_{xx}}{\sigma_{xx} + \sigma_{xy}} \simeq \frac{\sigma_{xx}}{\sigma_{xy}}$, where $\sigma_{xy} \simeq \frac{n_i e}{B}$ and $\sigma_{xx} \ll \sigma_{xy}$.

The expression of the conductivity σ_{xx} shows the physical equivalence to a situation with only one scattering time and two different oscillations frequencies for the MW-driven subbands: $w/3$ for the intra-band scattering and w for the inter. They demonstrate also the origin for the regular and strong interference profile observed in experiments where the factor $1/3$ is essential to obtain the interference effect. A different factor would produce a totally distinct interference and also distinct R_{xx} response. This factor comes from the calculation of the squared magnitude of the corresponding form factors F_{intra} and F_{inter} which eventually determine the different scattering rate between the intra-subband and the inter-one processes. These form factors depend mainly on the variational parameter b and on the averaged wave vector \bar{q} which subsequently are determined by two-dimensional impurity density n_i . Therefore we can conclude that the crucial parameter $1/3$ and eventually the obtained interference profile will be mainly dependent on n_i . During the scattering jump the electron *perceives* an approximately three times faster MW-driven oscillation of the 2DES when is inter-subband with respect to the intra-subband. This equation reflects also the important result that the intra-band conductivity (upper term in the σ_{xx} expression) is three times larger than the inter-subband (lower term of σ_{xx}). Then, the total current is mainly supported by intra-subband scattering processes regarding the inter processes in a relation of approximately three to one.

Based in these results, we can explain physically how the interference between both types of scattering process work, producing an excess of current at minima and a lack of current at maxima. In Fig. 2 we present schematic diagrams for the different situations. In all of them the MW field is on and the electronic orbits are not fixed, and instead move back and forth through x_{cl} . In Fig. 2a, the intra-subband scattering corresponds to a peak and the orbits moves backwards during the jump, then on average, electrons advance further than in the no MW case. Thus, we obtain more current giving rise to peaks because the average advanced distance is directly proportional to the conductivity. Yet, according to our calculations, only three out of four of the total scattering

processes take place through the intra-subband channel. The other one out of four are inter-subband processes (see Fig. 2b). In them, due to the slower scattering time (or higher w) the scattering jump occurs when the electronic orbits are moving forward. Therefore, the average advanced distance is smaller than in the intra processes. Eventually at the peaks, the total advanced distance, $\frac{3}{4}\Delta X_{intra}^{MW} + \frac{1}{4}\Delta X_{inter}^{MW}$, is smaller than the one-subband case. Accordingly, this is directly translated to the obtained current, being reflected in the narrower peaks profile (see Fig. 3b).

The valleys situation can be explained in similar terms as the peaks. Now, in the intra processes (see Fig. 2c) the scattering jump takes place when the electronic orbits are moving forward giving a smaller electronic advanced distance and current. This situation gives rise to valleys and eventually if the MW power is big enough the ZRS can be achieved. As before, these intra-subband scattering processes correspond to three out of four of the total (see Fig. 2c). The other one out of four develops through the inter-subband channel (see Fig. 2d). In these processes, again due to the smaller scattering time or higher w , the scattering jump occurs when the electronic orbits are going backwards giving rise to a larger average advanced distance and current (see Fig. 2d). Then, summing up all scattering processes we obtain more current than the one-subband case. This is the physical origin of the two shoulder that can be observed a both sides at minima of R_{xx} versus b .

III. RESULTS

In Fig. 3a, we present calculated R_{xx} vs B for dark and MW situations and frequency $f = w/2\pi = 143$ GHz. We can observe MISO for the no-MW curve, MIRO for the MW curve and the ZRS marked with an arrow. In Fig. 3b, we present the same as in 3a, but for 2-subbands and 1-subband cases. The later has been obtained making $\Delta_{12} \rightarrow 0$. Contrasting both curves we observe the new features appearing regularly spaced in peaks and valleys: two nearly symmetric shoulders in valleys and narrower peaks regarding the 1-subband curve. According to our model, these new features are result of the interference between the competing intra and inter-subband scattering processes. This interference effect is mainly based in the different scattering rates between intra and inter-subband scattering events. On the one hand this is going

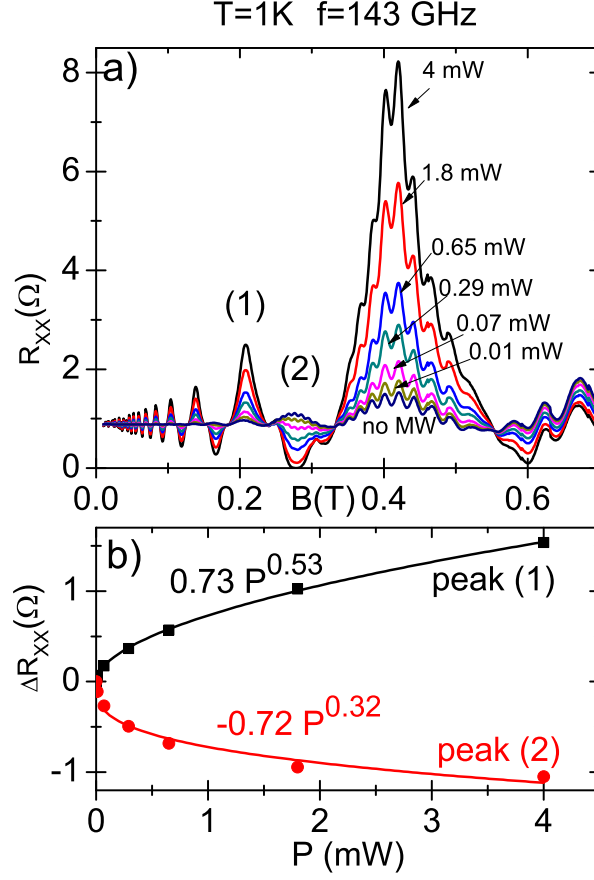


FIG. 5: a) Calculated results of power dependence of R_{xx} vs B . MW power decreases from 4 mW to darkness and MIRO's decrease too. This is a similar behavior as the 1-subband result. b) Calculated $\Delta R_{xx} = R_{xx}^{MW} - R_{xx}^0$ vs power, for data coming from peaks (1) and (2) of the upper panel. The obtained fits for both peaks mean a sublinear P -dependence in agreement with previous experimental²² and theoretical⁴¹ results.

to be obviously reflected in the different scattering times: the inter process is three times smaller than the intra-subband. On the other hand, in the different capability to support the current. The intra-subband processes are able to support three times more current than the inter. Thus, in valleys, we observe a constructive interference effect giving rise to two shoulders meaning more current through the sample, meanwhile the narrower peaks mean a destructive interference and less current. The presence of ZRS is explained similarly as in ref.⁵.

In Fig.4 we present calculated R_{xx} vs B for different MW frequencies. In 4a, for a lower frequencies range (from 50 to 100 GHz)⁴⁰ and in 4b, for a higher frequencies range (from 110 to 180 GHz)²³. We observe in all cases the presence of ZRS with shifting position depending on f and with reasonable agreement with experiment. All curves present the peaks and valley features meaning the importance of the interference effect which shows up independently of f . This f -dependence of ZRS positions was previously and similarly observed

in one-subband samples^{2,3}.

In Fig. 5a we present P -dependence of R_{xx} vs B for $f = 143\text{ GHz}$. We observe that MIRO's decrease as P , (and E_0), gets smaller from 4 mW to darkness in similar behavior as the 1-subband results². In 5b, we present $\Delta R_{xx} = R_{xx}^{MW} - R_{xx}^0$ vs P , for data coming from peaks (1) and (2) of Fig. 5a, where R_{xx}^0 is the magnetoresistance for darkness and R_{xx}^{MW} is the magnetoresistance when the MW field is on. We fit the data obtaining for both peaks a sublinear P -dependence, $R_{xx} \propto P^\alpha$ where $\alpha < 1$ and explained in terms of:

$$E_0 \propto \sqrt{P} \Rightarrow R_{xx} \propto \sqrt{P} \quad (22)$$

and in agreement with current²³ and previous experimental²² and theoretical⁴¹ results.

In Fig 6a. we present the T dependence of R_{xx} vs B for $f = 143\text{ GHz}$. As in 1-subband samples, we observe a clear decrease of MIRO for increasing T , eventually reaching a R_{xx} response similar to darkness. In Fig. 6b, we present $\ln \Delta R_{xx}$ vs $1/T$ for data coming from peaks

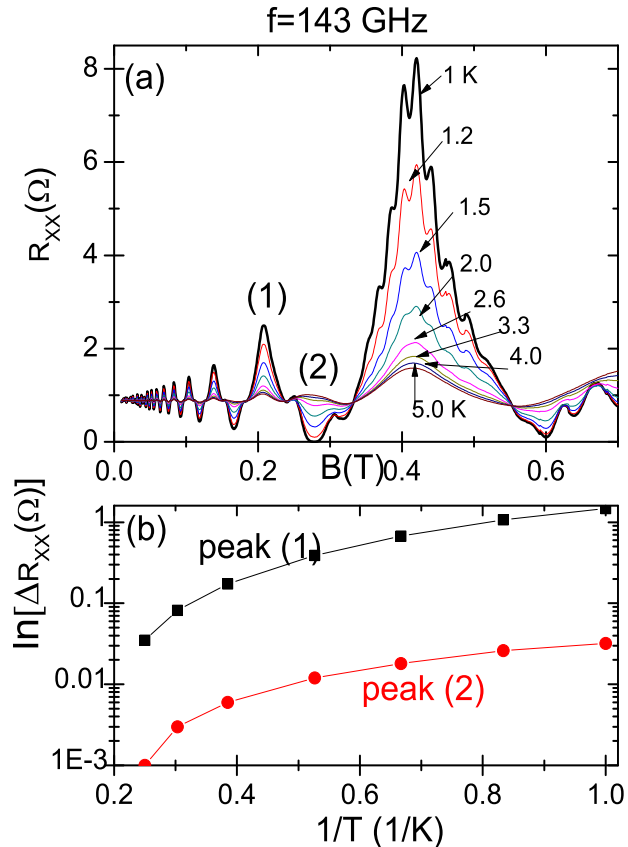


FIG. 6: a) Calculated results of T dependence of R_{xx} vs B for $f = 143$ GHz. As in 1-subband samples, we observe a clear decrease of MIRO for increasing T , eventually reaching a R_{xx} response similar to darkness. b) $\ln \Delta R_{xx}$ vs $1/T$ for data coming from peaks (1) and (2) of 6a. The fitted curves show the relation $R_{xx} \propto T^{-2}$ in agreement with experiment. The T -dependence is explained with the damping parameter γ which represents the interaction of electrons with acoustic phonons. γ is linear with $T^{5,32}$, thus an increasing T means an increasing γ and smaller MIRO's. When the damping is strong enough (higher T), MIRO's collapse

(1) and (2) of Fig. 6a. The T -dependence, according to the model, is explained with the damping parameter γ which represents the interaction of electrons with acoustic phonons. γ is linear with $T^{5,32}$, thus an increasing T means an increasing γ and smaller MIRO's. When the damping is strong enough (higher T) MIRO's collapse. The curves of Fig. 6b show the relation $R_{xx} \propto T^{-2}$ in agreement with experiment²³.

IV. CONCLUSIONS

In summary, we have theoretically studied the recently discovered microwave-induced resistance oscillations and zero resistance states in Hall bars with two occupied subbands. MW-driven magnetoresistance presents a peculiar shape which appears to have a built-in

interference effect not observed before. Applying the microwave-driven electron orbit model, we calculate different intra and inter-subband electron scattering rates under MW, revealing that the first is three times greater than the latter. This is physically equivalent to different microwave-driven oscillation frequencies for the two electronic subbands. Through scattering, these subband-dependent oscillation motions interfere giving rise to such a striking resistance profile. In the valleys the interference is constructive giving rise to two symmetric extra shoulders at each side of minima. In the peaks the interference is destructive producing smaller peaks regarding the one-subband case. The factor ~ 3 is essential to obtain this strong and regularly spaced interference effect. We study also the dependence on MW frequency, MW intensity and temperature. Calculated results are in good agreement with experiments.

V. ACKNOWLEDGMENTS

This work is supported by the MCYT (Spain) under grant: MAT2008-02626/NAN.

VI. REFERENCES

- ¹ J. Iñarrea, G. Platero and C. Tejedor, *Semicond. Sci. Tech.* **9**, 515, (1994); J. Iñarrea, G. Platero, *Phys. Rev. B*, **51**, 5244, (1995); *Europhys. Lett.* **34**, 43, (1996); *Europhys Lett.* **33**, 477, (1996); *Europhys Lett.* **40**, 417, (1997).
- ² R. G. Mani, J. H. Smet, K. von Klitzing, V. Narayana-murti, W. B. Johnson, and V. Umansky, *Nature(London)* **420**, 646 (2002); R. G. Mani, V. Narayanamurti, K. von Klitzing, J. H. Smet, W. B. Johnson, and V. Umansky, *Phys. Rev. B* **69**, 161306 (2004); *Phys. Rev. B* **70**, 153310 (2004).
- ³ M. A. Zudov, R. R. Du, L. N. Pfeiffer, and K. W. West, *Phys. Rev. Lett.* **90**, 046807 (2003).
- ⁴ S. A. Studenikin et al., *Sol. St. Comm.* **129**, 341 (2004).
- ⁵ J. Iñarrea and G. Platero, *Phys. Rev. Lett.* **94** 016806, (2005); J. Iñarrea and G. Platero, *Phys. Rev. B* **72** 193414 (2005); J. Iñarrea and G. Platero, *Appl. Phys. Lett.*, **89**, 052109, (2006); J. Iñarrea and G. Platero, *Phys. Rev. B*, **76**, 073311, (2007); J. Iñarrea, *Appl. Phys. Lett.* **90**, 172118, (2007)
- ⁶ A.C. Durst, S. Sachdev, N. Read, S.M. Girvin, *Phys. Rev. Lett.* **91** 086803 (2003)
- ⁷ C. Joas, J. Dietel and F. von Oppen, *Phys. Rev. B* **72**, 165323, (2005)
- ⁸ X.L. Lei, S.Y. Liu, *Phys. Rev. Lett.* **91**, 226805 (2003)
- ⁹ Ryzhii et al, *Sov. Phys. Semicond.* **20**, 1299, (1986)
- ¹⁰ P.H. Rivera and P.A. Schulz, *Phys. Rev. B* **70** 075314 (2004)
- ¹¹ Junren Shi and X.C. Xie, *Phys. Rev. Lett.* **91**, 086801 (2003)
- ¹² R. G. Mani et al., *Phys. Rev. Lett.* **92**, 146801 (2004).
- ¹³ R. G. Mani et al., *Phys. Rev. B* **69**, 193304 (2004).
- ¹⁴ R. L. Willett, L. N. Pfeiffer, and K. W. West, *Phys. Rev. Lett.* **93**, 026604 (2004).
- ¹⁵ R. G. Mani, *Physica E (Amsterdam)* **22**, 1 (2004);
- ¹⁶ J. H. Smet et al., *Phys. Rev. Lett.* **95**, 118604 (2005).
- ¹⁷ Z. Q. Yuan et al., *Phys. Rev. B* **74**, 075313 (2006).
- ¹⁸ K. Stone et al., *Phys. Rev. B* **76**, 153306 (2007).
- ¹⁹ S. I. Dorozhkin et al., *Phys. Rev. Lett.* **102**, 036602 (2009).
- ²⁰ A. T. Hatke et al., *Phys. Rev. Lett.* **102**, 086808 (2009).
- ²¹ R. G. Mani et al., *Phys. Rev. B* **79**, 205320 (2009).
- ²² R. G. Mani et al., *Phys. Rev. B* **81**, 125320, (2010).
- ²³ S. Wiedmann, G.M. Gusev, O.E. Raichev, A.K. Bakarov, and J.C. Portal, *Phys. Rev. Lett.*, **105**, 026804, (2010)
- ²⁴ S. Wiedmann, G.M. Gusev, O.E. Raichev, A.K. Bakarov, and J.C. Portal, *Phys. Rev. B*, **81**, 085311, (2010); S. Wiedmann, N.C. Mamani, G.M. Gusev, O.E. Raichev, A.K. Bakarov, and J.C. Portal, *Phys. Rev. B*, **80**, 245306, (2009); S. Wiedmann, G.M. Gusev, O.E. Raichev, T.E. Lamas, A.K. Bakarov, and J.C. Portal, *Phys. Rev. B*, **78**, 121301, (2008);
- ²⁵ D. Konstantinov and K. Kono, *Phys. Rev. Lett.* **103**, 266808 (2009)
- ²⁶ D. Konstantinov and K. Kono, *Phys. Rev. Lett.* **105**, 226801 (2010)
- ²⁷ S. I. Dorozhkin, L. Pfeiffer, K. West, K. von Klitzing, J.H. Smet, *NATURE PHYSICS*, **7**, 336-341, (2011)
- ²⁸ O. E. Raichev, *Phys. Rev. B* **78**, 125304 (2008); N. C. Mamani, G. M. Gusev, O. E. Raichev, T. E. Lamas, and A. K. Bakarov, *Phys. Rev. B* **80**, 075308 (2009).
- ²⁹ R. G. Mani, *Int. J. Mod. Phys. B*, **18**, 3473, (2004); *Physica E*, **25**, 189 (2004)
- ³⁰ M. A. Zudov, R. R. Du, L. N. Pfeiffer, and K. W. West, *Phys. Rev. Lett.* **96**, 236804 (2006)
- ³¹ *Phys. stat. sol. (a)*, **204**, 467, (2007)
- ³² J. Inarrea and G. Platero, *Appl. Phys Lett.* **89**, 172114, (2006)
- ³³ E.H. Kerner, *Can. J. Phys.* **36**, 371 (1958) .
- ³⁴ K. Park, *Phys. Rev. B* **69** 201301(R) (2004).
- ³⁵ J. Iñarrea and G. Platero, *Appl. Phys Lett.* **93**, 062104, (2008); J. Iñarrea and G. Platero, *Phys. Rev. B.* **78**, 193310, (2008); J. Iñarrea, *Appl. Phys Lett.* **92**, 192113, (2008); Jesus Inarrea and Gloria Platero, *Appl. Phys. Lett.* **95**, 162106, (2008); J. Iñarrea, G. Platero and C. Tejedor, *Semicond. Sci. Tech.* **9**, 515, (1994); J. Iñarrea, G. Platero, *Phys. Rev. B*, **51**, 5244, (1995); *Europhys. Lett.* **34**, 43, (1996); *Europhys Lett.* **33**, 477, (1996); *Europhys Lett.* **40**, 417, (1997).
- ³⁶ B.K. Ridley. *Quantum Processes in Semiconductors*, 4th ed. Oxford University Press, (1993).
- ³⁷ T. Ando, A. Fowler and F. Stern, *Rev. Mod. Phys.*, **54**, (1982).
- ³⁸ John H. Davies, *The Physics of Low-dimensional Semiconductors*, Cambridge University Press, (1997).
- ³⁹ V. Mitin, V.A. Kochelap and M.A. Stroschio. *Quantum Heterostructures*, Cambridge University Press, (1999).
- ⁴⁰ S. Wiedmann, G. M. Gusev, O. E. Raichev, A. K. Bakarov, and J. C. Portal, *Proceedings of the 19th International Conference on the Application of High Magnetic Fields in Semiconductor Physics (HMF-19)*, Fukuoka, Japan, 2010 (unpublished)
- ⁴¹ Jesus Inarrea, R.G. Mani and W. Wegscheider, *Phys. Rev.* **82** 205321 (2010); R. G. Mani, C. Gerl, S. Schmult, W. Wegscheider, V. Umansky, *Phys. Rev. B* **81**, 125320 (2010).